INFORMATICS JOURNALS
The Journal of Electrochemical Society of India, Volume 75, Issue (1&2), January-March 2026; pp. 45–56
ISSN (Print) : 0013-466X
ISSN (Online) : xxxx-xxxx
DOI: 10.18311/JESCI/2026/75218

Magsure Zn-Al-Mg Coating: Superior Corrosion Resistance and Formability

H. K. Mehtani*, Vineet Patel, Vivek Kumar Yadav, K. M. Sampath Swamy, Sandeep Kushwaha and D. Satish Kumar

JSW Steel Limited, Vijayanagar Works, Bellary District – 583275, Karnataka, India

Abstract

Magsure is an advanced Zn–Al–Mg hot-dip alloy coating designed for structural-grade steel requiring superior corrosion resistance without compromising formability. In this study, Magsure coatings were produced at 80, 120, 275, and 450GSM, and their microstructure and corrosion behaviour were investigated. Scanning Electron Microscopy-Energy Dispersive Spectroscopy (SEM–EDS) and X-Ray Diffraction (XRD) analyses confirmed the presence of $MgZn_2$ intermetallic phases distributed within the coating microstructure, with a phase fraction of 21–27 vol%, contributing to enhanced corrosion protection through combined sacrificial and barrier effects. To establish industrial relevance, a direct comparison was made between GI 275GSM and Magsure 275GSM. Formability tests, including cupping, drawing, and Hole Expansion Ratio (HER), showed that Magsure 275GSM retained formability comparable to conventional GI 275 GSM, with no major loss in forming performance. In contrast, corrosion testing by neutral salt spray, cyclic corrosion exposure, and electrochemical impedance spectroscopy revealed a pronounced increase in corrosion life for Magsure 275 GSM relative to GI 275 GSM. The results demonstrate that the Zn–Al–Mg coating system delivers a significant improvement in corrosion durability while preserving the formability required for practical fabrication, making Magsure a strong candidate for high-durability applications in aggressive service environments.

Keywords: Bending, Cupping, Electrochemical, Hot-Dip Galvanising, Magsure, Salt Spray Testing (SST), Zn-$MgZn_2$

1. Introduction

Hot-dip galvanising is one of the most widely adopted surface engineering routes for protecting steel against corrosion. By providing both barrier protection and sacrificial cathodic protection, zinc-based coatings significantly enhance the service life of steel components exposed to aggressive environments. From a sustainability perspective, improved corrosion protection reduces premature material failure, thereby minimising the frequency of equipment replacement, maintenance requirements, and associated resource consumption[1,2].

Among zinc-based protective systems, Zn-Al-Mg coatings are advanced protective coated steel substrates to provide enhanced corrosion resistance and mechanical durability compared to conventional zinc or zinc-aluminium coatings. These coatings are usually manufactured by hot-dip galvanising techniques and have gained significant interest in many industries, including construction, automotive, and household appliances, due to their superior corrosion performance in harsh environments[3,4]. This superior corrosion resistance is because the synergistic presence of Al and Mg contributes to the formation of dense, stable corrosion products such as simonkolleite ($Zn_5[OH]_8Cl_2{\cdot}H_2O$) and layered double hydroxides (Zn-Al layered double hydroxide (Zn-Al LDH)), which impart enhanced barrier properties and retard localised corrosion mechanisms at exposed steel sites[5,6].

Previous studies have highlighted the critical role of magnesium in improving the corrosion performance of Zn-based alloy coatings. Rai *et al.* reported that Zn–5Al coatings containing 4.5 wt.% Mg exhibited nearly twice the corrosion resistance of coatings containing 1.5 wt.%

*Email: hitesh.kumar@jsw.in

Mg, and approximately an order of magnitude higher resistance than conventional galvanised coatings. This improvement was attributed to the beneficial galvanic interactions associated with the sacrificial $MgZn_2$ phase, which plays an important role in corrosion protection[7]. Similarly, Volovitch *et al*. investigated the effect of Mg addition in Zn–Mg coatings and observed that both Zn and Zn–Mg coatings initially formed simonkolleite during the early stages of corrosion. However, upon prolonged exposure, simonkolleite disappeared in coatings without magnesium, whereas Mg-containing coatings retained more compact and protective corrosion products, thereby improving long-term corrosion resistance[6].

For conventional galvanised coatings, corrosion life is generally governed by coating thickness, as protection of the underlying steel is primarily provided through the sacrificial consumption of zinc. In contrast, the corrosion resistance of Zn–Al–Mg coatings is influenced by alloy chemistry, solidification microstructure, and exposure conditions. Recent studies have shown that Mg-rich intermetallics, particularly $MgZn_2$, facilitate the formation of stable protective corrosion products, while cooling rate, coating weight, and cut-edge exposure significantly affect eutectic morphology, crack susceptibility, and long-term durability in aggressive environments[8–14]. In contrast, the corrosion behaviour of Zn–Al–Mg coatings are more complex due to the presence of multiple microstructural constituents with distinct electrochemical potentials[15-18]. These heterogeneous phases can induce localised micro-galvanic interactions within the coating itself, thereby influencing corrosion initiation, corrosion product evolution, and the overall degradation mechanism. Consequently, in Zn–Al–Mg systems, not only the total coating thickness but also the phase constitution, phase morphology, and through-thickness distribution of microstructural features are expected to play a decisive role in determining corrosion performance[19-20].

In this context, the present study focuses on Magsure, an advanced Zn–Al–Mg hot-dip alloy-coated steel system, developed to achieve enhanced corrosion resistance over a broad range of coating mass thicknesses (80, 120, 300, and 450GSM) for construction-grade applications. Particular emphasis is placed on understanding the relationship between coating microstructure, phase constitution, and corrosion behaviour, with special attention to the role of $MgZn_2$ intermetallic phases in improving the protective response of the coating. To establish its industrial relevance, the performance of Magsure 275GSM was directly compared with that of conventional GI 275GSM in terms of both corrosion resistance and formability. Formability assessment through cupping, drawing, and HER was undertaken to determine whether the improved corrosion performance of the Zn–Al–Mg coating is achieved without compromising processing characteristics. By correlating microstructural features with electrochemical and accelerated corrosion behaviour, this study aims to demonstrate that while Magsure 275GSM exhibits formability comparable to GI 275GSM, it provides a substantially longer corrosion life. Such a balance between manufacturability and durability makes Magsure a promising coating solution for roofing, cladding, and other long-life structural applications in aggressive marine and industrial environments.

2. Methodology

2.1 Sample Preparations of Zn-Al-Mg Coated Steel

The hot-dip Zn–Al–Mg alloy-coated steel sheets (Magsure (Zn–Al–Mg coating, in which the composition is typically in the range of 4–5 wt.% Mg and 4–5 wt.% Al, with the balance Zn)) investigated in the present work were industrially produced at JSW Steel Coated Products. Four coating masses, namely 80, 120, 275, and 450GSM, corresponding to average coating thicknesses of 8.0082 ± 0.35µm, 10.2005 ± 0.32µm, 24.462 ± 0.53µm, and 45.052 ± 0.62µm, respectively, were selected for the study. Samples were sectioned from the coated sheets using a mechanical shearing process. Specimens of 25mm × 25mm were prepared for SEM–EDS, XRD, and electrochemical characterisation, including Electrochemical Impedance Spectroscopy (EIS) and potentiodynamic polarisation measurements. For accelerated corrosion testing, specimens of 90mm × 90mm were prepared for salt spray exposure. Microstructural characterisation was first performed on all four Magsure coating masses to evaluate the influence of coating mass on morphology and phase constitution. Based on this, the later part of the study focused on a comparative evaluation of GI and Magsure coatings in terms of corrosion resistance and formability. The comparative assessment included SST, cyclic corrosion testing after deformation by cupping, drawing, and HER, corrosion testing in a concrete medium, and electrochemical polarisation analysis.

2.2Microstructural Characterisation of Magsure Coatings

Sheared coupons of dimensions 25mm × 25mm were ultrasonically cleaned in acetone using a BRANSON 2800 unit to remove oil, dirt, and other surface contaminants prior to analysis. Microstructural characterisation was performed using a Thermo Fisher Quanta 600TM scanning electron microscope.

For surface examination, the cleaned coated specimens of different GSM were directly loaded into the SEM chamber and analysed in the as-received condition. For cross-sectional analysis, the cleaned samples were mounted vertically using metallic holding clips and hot mounted in acrylic resin with a Struers CitoPress-15 mounting system. The mounted specimens were successively ground using 600, 800, 1000, 1200, and 1500 grit SiC papers, followed by fine polishing using 0.1µm diamond paste in a Struers Tegramin-20 automatic polishing machine operated at 200rpm under a 10N load for 30 min to obtain a mirror-finished cross-section. The polished samples were cleaned with acetone, dried, gold sputter-coated using a Quorum sputter coater, and subsequently examined under SEM.

Elemental analysis of the coating and phase constituents was carried out by Energy-Dispersive X-ray Spectroscopy (EDS) using an attached Bruker™ EDS detector.

2.3 Phase Analysis by X-ray Diffraction

The phase constitution of the coated steel was evaluated by X-ray Diffraction (XRD) for two representative coatings, namely GI 275 and Magsure 275. Coupons of dimensions 25mm × 25mm were ultrasonically cleaned in acetone prior to analysis to ensure removal of surface contaminants. The cleaned specimens were then mounted on a PANalytical Empyrean X-ray diffractometer (Malvern Panalytical™) for phase characterisation.

XRD measurements were carried out using Cu Kα radiation ($\lambda \approx 1.54$ A˚), and diffraction data were collected over a 2θ range of 10° to 90°. The recorded diffraction patterns were analysed to identify the crystalline phases present in the coatings and to compare the phase constitution of the conventional GI 275 coating with that of the Zn–Al–Mg-based Magsure 275 coating.

2.4 Salt Spray and Cyclic Corrosion Testing of GI and Magsure Coatings

The accelerated corrosion performance of GI 275 and Magsure 275 coatings was investigated using neutral SST and CCT. For salt spray exposure, coated specimens of dimensions 90mm × 90mm were shear-cut from the coated sheets and cleaned with acetone before testing. To suppress premature corrosion initiation from geometrical discontinuities, the corners of the specimens were sealed to reduce the corner effect. The prepared specimens were then exposed in an Ascott™ CC450ip series corrosion chamber under neutral salt spray conditions in accordance with American Society for Testing and Materials (ASTM) B117. Observations were recorded at 24 h intervals, and the corrosion behaviour was assessed based on the onset and progression of white rust, red rust, and overall coating degradation.

To evaluate the influence of forming-induced strain on corrosion performance, separate sets of GI 275 and Magsure 275 specimens were deformed by cupping, HER, and drawing tests before corrosion exposure. These pre-deformed specimens were subsequently subjected to cyclic corrosion testing under the selected ASTM-based exposure protocol. The corrosion response of the deformed zones was then examined and compared in order to determine the ability of both coating systems to retain corrosion resistance after mechanical deformation.

2.5 Corrosion Test in Concrete Structure

The corrosion performance of GI 275 and Magsure 275 coatings in a concrete environment was assessed by embedding the coated specimens in M40-grade concrete and subsequently exposing them to chloride-rich conditions. Rectangular coupons of dimensions 80mm × 50mm were prepared from the coated sheets. Before embedding, all specimens were cleaned with acetone, rinsed with deionised water, air dried, and weighed to an accuracy of ±0.001g.

Each specimen was placed vertically at the centre of one face of a 75mm × 75mm × 75mm steel mould containing freshly cast M40 concrete, such that approximately 80% of the specimen length was embedded in concrete and 20% remained exposed. Non-corrodible spacers were used to ensure precise alignment and placement of the specimens during casting. The moulds were stored in a humidity chamber maintained at 27°C and 95% RH for 24 h, after which the concrete cubes were demoulded and cured in water at 25 ± 2°C for 28 days.

The concrete was prepared in accordance with IS 456 and IS 516 using Ordinary Portland Cement (OPC), manufactured sand, coarse aggregate, water, and suitable admixtures. Details of the mix design are provided in the

Supporting Information. Following curing, the concrete-embedded specimens were exposed to 3.5 wt.% NaCl solution/environment to accelerate chloride ingress and corrosion. The comparative corrosion behaviour of GI275 and Magsure 275 under simulated concrete service conditions was then evaluated.

3. Results and Discussion

3.1 Microstructural Evolution of Zn–Al–Mg Coatings with Coating Mass

Figure 1 presents the SEM micrographs showing the phase morphology of the Zn–Al–Mg-coated steel at different coating masses. Figures 1(a), (c), (e), and (g) show the surface morphologies of the 80, 120, 275, and 450GSM coatings, respectively, whereas Figures 1(b), (d), (f), and (h) show the corresponding cross-sectional morphologies.

At 80GSM, the coating exhibits a relatively fine and homogeneous microstructure, dominated by a finely distributed binary eutectic Zn–$MgZn_2$ phase. The finer scale of this eutectic morphology is attributed to the higher cooling rate associated with the lower coating thickness. As the coating mass increases to 120GSM, the eutectic structure becomes relatively coarser, and the emergence of the primary $MgZn_2$ phase is observed along with the presence of ternary eutectic regions of Zn–$MgZn_2$–Al. The development of these additional eutectic constituents indicates progressive microstructural evolution with increasing coating thickness.

A further increase in coating mass to 275 and 450GSM leads to more pronounced coarsening of the eutectic structure. The binary Zn–$MgZn_2$ eutectic becomes wider and less refined, while the fraction and size of the primary $MgZn_2$ phase increase. In addition, the ternary Zn–$MgZn_2$–Al eutectic becomes more evident at higher coating masses. This progressive coarsening is consistent with the lower solidification rate associated with thicker coatings. Thus, the SEM observations clearly indicate that coating mass strongly influences phase morphology, eutectic refinement, and phase distribution across the Zn–Al–Mg coating.

To verify the chemical constitution of the phases observed in the SEM micrographs, EDS analysis was performed, as shown in Figure 2. The EDS results support the phase identification and reveal the variation in phase constitution with increasing coating mass.

For the 80GSM coating, shown in Figure 2(a), the microstructure is primarily composed of primary Al-rich dendritic regions and binary Zn–$MgZn_2$ eutectic phase distributed across the coating cross-section. The predominance of these relatively fine features is consistent with the rapid cooling associated with the thinner coating. For the 120GSM coating, shown in Figure 2(b), three distinct constituents become more evident throughout the cross-section, namely primary $MgZn_2$, binary Zn–$MgZn_2$ eutectic, and ternary Zn–$MgZn_2$–Al eutectic,

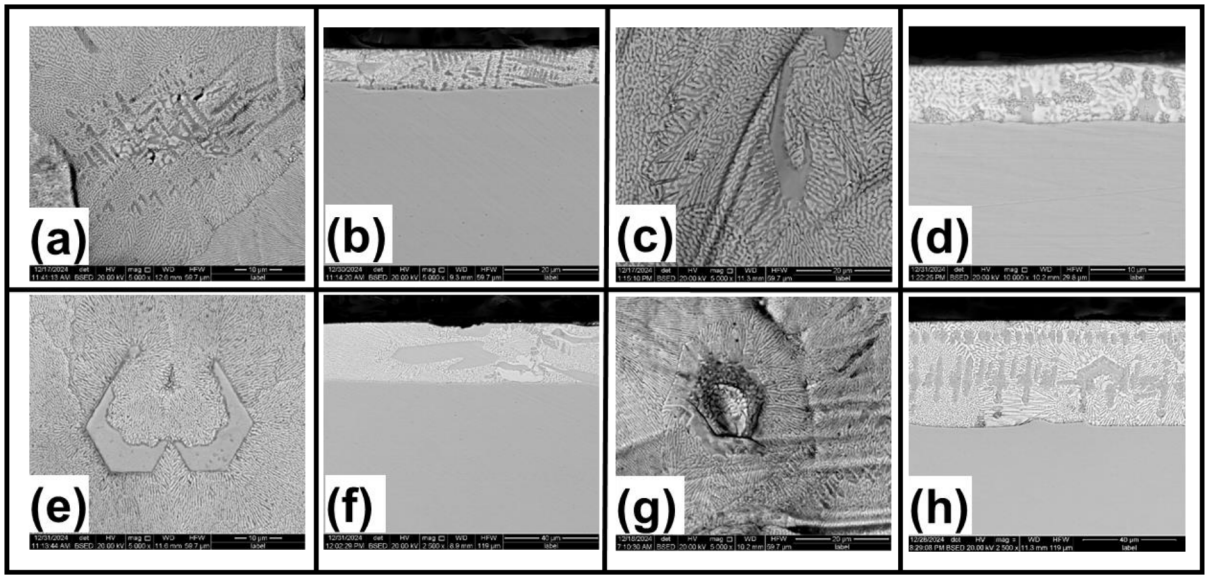
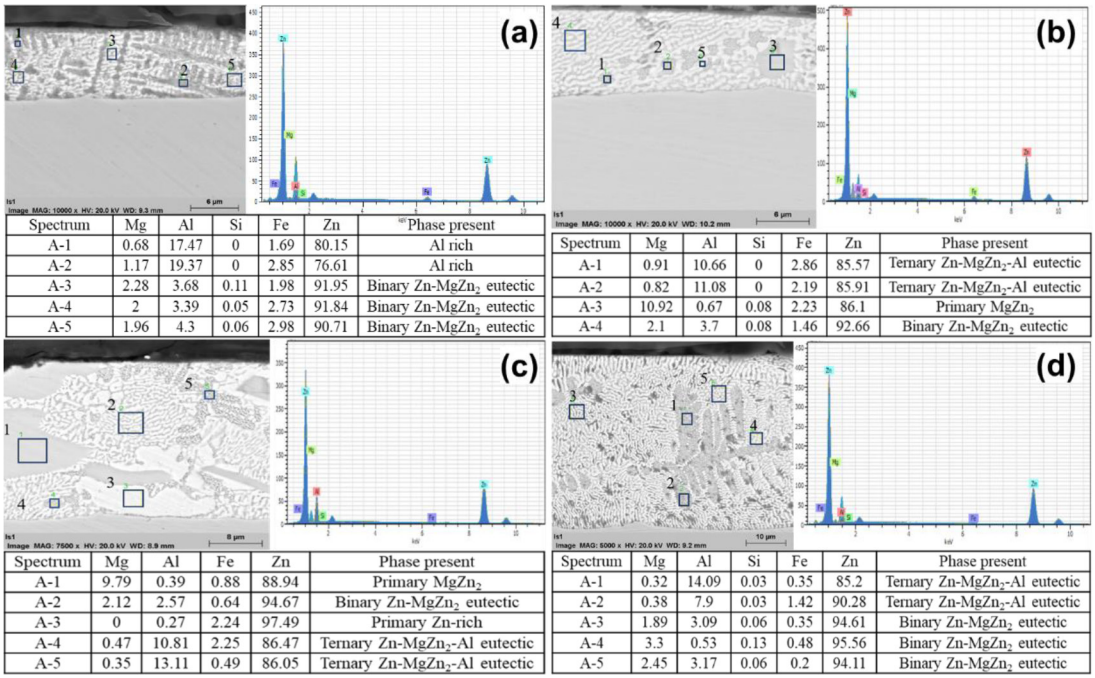


Figure 1. SEM micrographs of (a, c, e, g) surface and (b, d, f, h) cross-section morphologies of samples with 80, 120, 275, and 450GSM, respectively.



Spectrum	Mg	Al	Si	Fe	Zn	Phase present
A-1	0.68	17.47	0	1.69	80.15	Al rich
A-2	1.17	19.37	0	2.85	76.61	Al rich
A-3	2.28	3.68	0.11	1.98	91.95	Binary Zn-$MgZn_2$ eutectic
A-4	2	3.39	0.05	2.73	91.84	Binary Zn-$MgZn_2$ eutectic
A-5	1.96	4.3	0.06	2.98	90.71	Binary Zn-$MgZn_2$ eutectic

Spectrum	Mg	Al	Si	Fe	Zn	Phase present
A-1	0.91	10.66	0	2.86	85.57	Ternary Zn-$MgZn_2$-Al eutectic
A-2	0.82	11.08	0	2.19	85.91	Ternary Zn-$MgZn_2$-Al eutectic
A-3	10.92	0.67	0.08	2.23	86.1	Primary $MgZn_2$
A-4	2.1	3.7	0.08	1.46	92.66	Binary Zn-$MgZn_2$ eutectic

Spectrum	Mg	Al	Fe	Zn	Phase present
A-1	9.79	0.39	0.88	88.94	Primary $MgZn_2$
A-2	2.12	2.57	0.64	94.67	Binary Zn-$MgZn_2$ eutectic
A-3	0	0.27	2.24	97.49	Primary Zn-rich
A-4	0.47	10.81	2.25	86.47	Ternary Zn-$MgZn_2$-Al eutectic
A-5	0.35	13.11	0.49	86.05	Ternary Zn-$MgZn_2$-Al eutectic

Spectrum	Mg	Al	Si	Fe	Zn	Phase present
A-1	0.32	14.09	0.03	0.35	85.2	Ternary Zn-$MgZn_2$-Al eutectic
A-2	0.38	7.9	0.03	1.42	90.28	Ternary Zn-$MgZn_2$-Al eutectic
A-3	1.89	3.09	0.06	0.35	94.61	Binary Zn-$MgZn_2$ eutectic
A-4	3.3	0.53	0.13	0.48	95.56	Binary Zn-$MgZn_2$ eutectic
A-5	2.45	3.17	0.06	0.2	94.11	Binary Zn-$MgZn_2$ eutectic

Figure 2. Energy-dispersive X-ray spectroscopy (EDS) spectra of Zn-Al-Mg coated steel samples of different coating weights: **(a)** 80 GSM, **(b)** 120 GSM, **(c)** 275 GSM, and **(d)** 450 GSM, showing elemental composition and distribution of phases within the coatings.

with the binary eutectic occupying a comparatively larger area fraction.

In the case of the 275GSM coating, shown in Figure 2(c), all major phases remain present, but the microstructure becomes noticeably coarser. This coarsening is reflected in the increased size of the primary intermetallic regions and the broader eutectic domains. Such coarsening can be attributed to the reduced cooling rate during solidification, which is commonly associated with lower line speeds used to obtain higher coating masses in industrial hot-dip processing. A similar trend is observed for the 450GSM coating, shown in Figure 2(d), where all major phases are retained, together with a further increase in the area fraction of the ternary Zn–$MgZn_2$–Al eutectic.

Figure 3 compares the surface morphology, cross-sectional microstructure, and microhardness of GI 275 and Magsure 275 coatings. A clear distinction is observed between the two coating systems at both the surface and cross-section levels.

The surface micrograph of GI 275 shows a relatively smooth and featureless morphology, characteristic of a conventional zinc coating with limited phase contrast. In contrast, the Magsure 275 surface exhibits a highly developed lamellar and eutectic-like morphology, indicating the presence of multiple solidification constituents within the Zn–Al–Mg alloy coating. This refined and heterogeneous surface structure is consistent with the formation of intermetallic and eutectic phases in the alloyed coating, which are absent in the simpler GI coating.

A similar difference is evident in the cross-sectional micrographs. The GI 275 cross-section appears comparatively uniform, with a relatively plain coating structure and finely dispersed features within the coating layer. On the other hand, the Magsure 275 cross-section reveals a distinctly multiphase microstructure composed of coarse and fine eutectic regions distributed throughout the coating thickness. The complex morphology of the Magsure coating indicates phase segregation during solidification and the development of Zn-rich and Mg/Al-containing eutectic constituents. Such a heterogeneous microstructure is expected to play an important role in corrosion protection by promoting preferential sacrificial dissolution of the more active Mg-containing phases and by facilitating the formation of stable corrosion products during exposure.

The difference in coating architecture is also reflected in the hardness values. GI 275 shows a microhardness in the range of 60–65HV (200g load), whereas Magsure

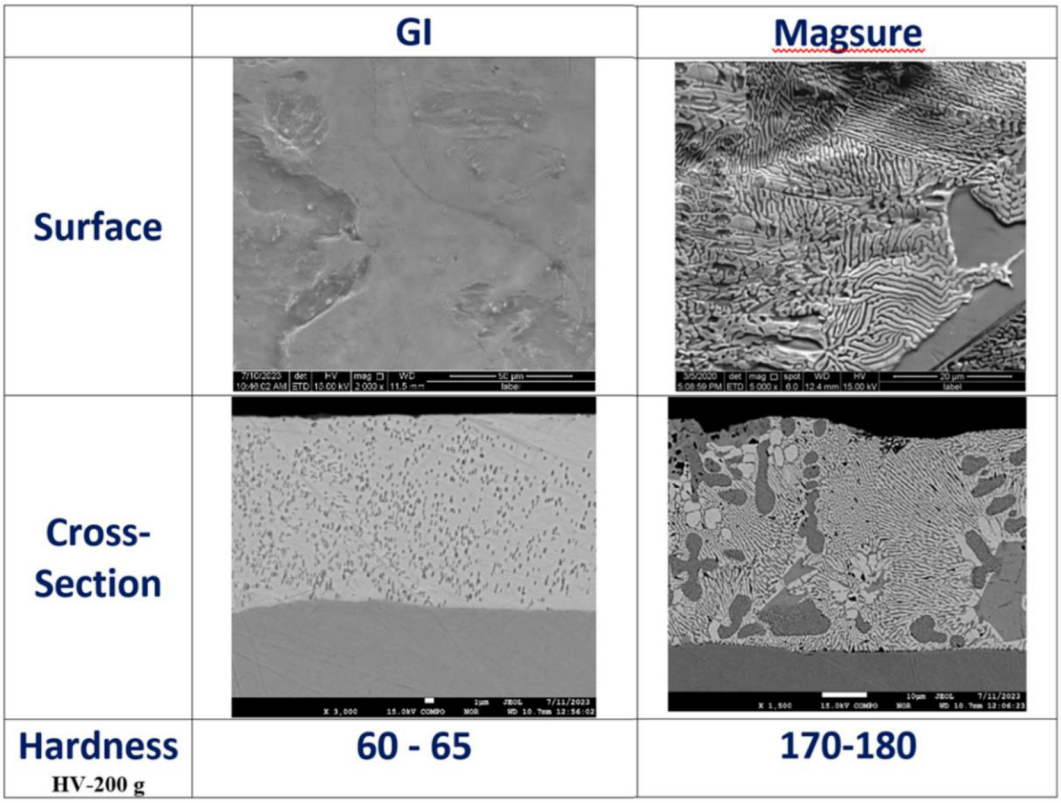


Figure 3. SEM comparison of GI 275 and Magsure 275 coatings showing surface morphology, cross-sectional microstructure and hardness.

275 exhibits a significantly higher hardness of 170–180 HV (200g load). The substantial increase in hardness for Magsure is attributed to its multiphase alloyed microstructure and the presence of hard intermetallic/eutectic constituents. Despite this higher hardness, the coating is intended to retain acceptable formability while providing markedly improved durability compared with GI.

Overall, Figure 3 demonstrates that, unlike GI 275, which possesses a comparatively simple zinc coating morphology, Magsure 275 exhibits a complex multiphase eutectic microstructure with substantially higher hardness. This microstructural difference is expected to be a key factor governing the superior corrosion resistance of the Zn–Al–Mg alloy-coated system.

3.2 Phase Analysis Through XRD

Figure 4 presents the X-ray diffraction patterns of GI 275 and Magsure 275 coatings. The diffraction pattern of GI 275 is predominantly characterised by peaks corresponding to the Zn-rich phase, which is typical of conventional galvanised coatings having a relatively simple phase constitution. In contrast, the diffraction pattern of Magsure 275 exhibits a more complex multiphase character, with distinct reflections corresponding to Zn-rich phases, Al-containing constituents, and the intermetallic $MgZn_2$ phase. The presence of $MgZn_2$ confirms the alloyed Zn–Al–Mg nature of the Magsure coating and is consistent with the lamellar and eutectic microstructure observed in the SEM analysis.

The phase quantification was carried out using HighScore analysis, which indicated that the $MgZn_2$ phase fraction in Magsure 275 lies in the range of 26–29%. This substantial fraction of Mg-containing intermetallic phase is expected to play a critical role in the corrosion behaviour of the coating. Owing to its electrochemical activity relative to the Zn-rich matrix, $MgZn_2$ can preferentially dissolve under corrosive exposure, thereby providing localised sacrificial protection and contributing to the improved corrosion resistance of the coating. In addition, the presence of a significant $MgZn_2$ fraction promotes the formation of compact and stable corrosion products, which further enhance the barrier properties of the Magsure coating.

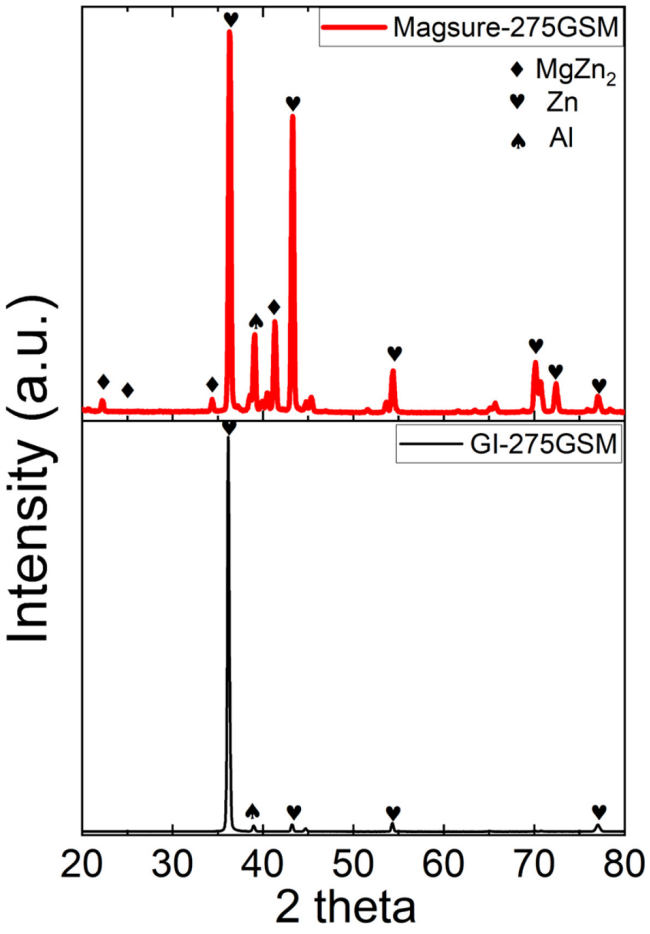


Figure 4. XRD patterns of GI 275 and Magsure 275 coatings showing the predominance of Zn in GI and the presence of $MgZn_2$ intermetallic phase in Magsure. Highscore analysis indicated that the $MgZn_2$ phase fraction in Magsure 275 is approximately 26–29%.

Overall, the XRD results demonstrate that, unlike GI 275, which is primarily composed of a Zn-dominant coating, Magsure 275 possesses a multiphase Zn–Al–Mg alloy structure containing a significant fraction of $MgZn_2$ intermetallic phase. This phase constitution is one of the key microstructural factors responsible for the superior corrosion performance of the Magsure coating.

3.3 Accelerated Corrosion Behaviour under Salt Spray Exposure

Figure 5 compares the salt spray corrosion response of GI 275 and Magsure 275 coatings under ASTM B117 exposure. A clear difference in corrosion progression is observed between the two coating systems. In the case of GI 275, visible white corrosion products became visible after ~500 h of exposure and by 960 h, the coating had already shown the onset of red rust, indicating breakdown of the sacrificial zinc layer and exposure of the steel substrate. In contrast, Magsure 275 exhibited markedly delayed corrosion progression throughout the test duration. White corrosion products were first observed only after approximately 4000h and even after 4272 h of salt spray exposure, the Magsure coating did not show red rust, with the surface remaining predominantly covered with white corrosion products.

This behaviour demonstrates the significantly improved durability of the Zn–Al–Mg-based Magsure coating compared with conventional GI of the same coating mass. Based on the experimental observation that GI showed red rust at 960 h, whereas Magsure remained free from red rust even at 4272 h, the corrosion life of Magsure can be considered to be at least 4.45 times higher than that of GI under the present test conditions. Since red rust was still absent in Magsure even at the end of the exposure period, the actual corrosion life enhancement is expected to be greater than 5 times. The delayed degradation of Magsure can be attributed to the presence of Mg-containing intermetallic and eutectic phases, which promote preferential sacrificial action and facilitate the formation of stable, protective corrosion products, thereby reducing the overall corrosion rate. Similar observations (impact of Mg on corrosion) have also been reported by other researchers[19].

Overall, the salt spray results clearly establish that Magsure 275 provides substantially longer corrosion life than GI 275, while maintaining the integrity of the coating for a much longer duration under chloride-rich accelerated exposure.

3.4 Corrosion Performance after Forming-Induced Deformation

To evaluate the corrosion durability of the coatings under forming-induced strain conditions, GI 275 and Magsure 275 specimens subjected to cupping, drawing, and hole expansion tests were further exposed to CCT. The deformed regions represent critical locations in practical applications, since local stretching, coating thinning, and strain concentration can accelerate coating breakdown and promote early corrosion initiation. The comparative corrosion response of the two coatings after 21, 42, and 72 cycles is shown in Figures 6 and 7.

In the cupping test, both coatings were initially intact before CCT exposure. After 21 cycles, GI 275 showed

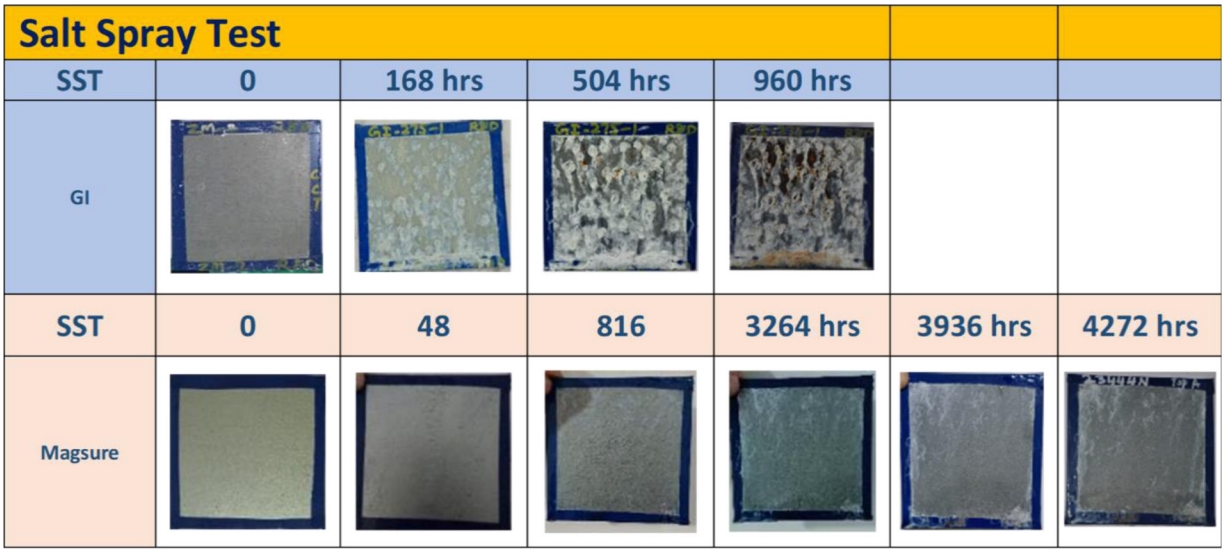


Figure 5. Comparative salt spray corrosion behaviour of GI 275 and Magsure 275 coatings under ASTM B117 exposure.

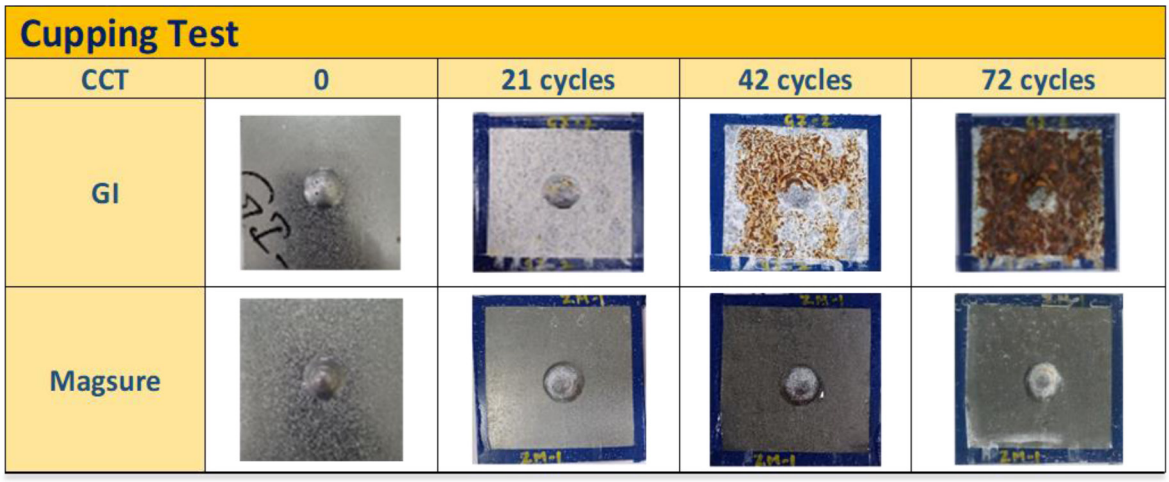


Figure 6. Comparative cyclic corrosion behaviour of GI 275 and Magsure 275 after cupping deformation, showing the surface condition before exposure and after 21, 42, and 72 CCT cycles. GI 275 exhibits rapid corrosion progression with extensive rusting at higher cycle numbers, whereas Magsure 275 retains significantly better surface protection throughout the test.

the formation of white corrosion products around the deformed dome region, indicating early degradation of the zinc coating. With further exposure to 42 cycles, significant corrosion progression was observed, with extensive rust formation over the specimen surface. By 72 cycles, the GI coating exhibited severe red rust, confirming breakdown of the protective coating and exposure of the steel substrate. In contrast, Magsure 275 showed only limited surface degradation throughout the test period. Even after 72 cycles, the deformed cupped region remained largely protected, with no comparable extent of red rust formation as observed in GI. This indicates that Magsure retains its corrosion protection much more effectively than GI, even under localised biaxial deformation.

A similar trend was observed in the drawing test. For GI 275, white corrosion products appeared after 21 cycles, followed by the development of localised red rust at 42 cycles and extensive rusting by 72 cycles. The drawn geometry, which introduces continuous deformation across the formed profile, appears to accelerate the failure of the conventional GI coating during cyclic exposure. By comparison, Magsure 275 exhibited markedly lower corrosion severity at all stages of exposure. Although some surface discolouration and corrosion-product formation were observed, the

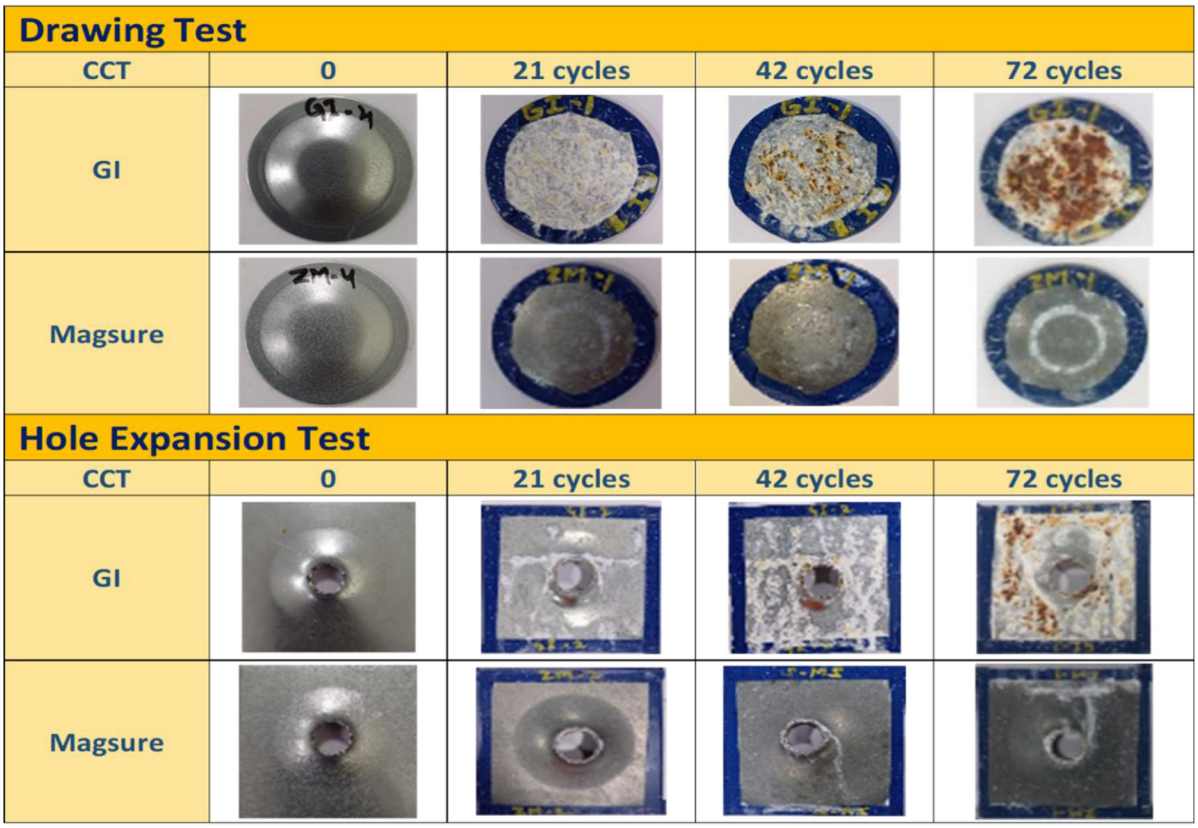


Figure 7. Comparative cyclic corrosion behaviour of GI 275 and Magsure 275 after drawing deformation and hole expansion testing, showing the surface condition before exposure and after 21, 42, and 72 CCT cycles. In both deformation modes, GI 275 shows earlier and more severe corrosion damage, whereas Magsure 275 exhibits markedly delayed degradation and improved corrosion resistance.

coating remained substantially intact even after 72 cycles, demonstrating a much slower degradation rate than GI under drawn deformation conditions.

The superiority of Magsure 275 is further evident in the hole expansion test, where the edge of the expanded hole acts as a highly strained and mechanically damaged region that is particularly vulnerable to corrosion initiation. In the case of GI 275, corrosion products developed rapidly around the hole edge, and red rust became increasingly pronounced with increasing CCT cycles. By 72 cycles, substantial degradation was visible around the expanded hole as well as on the surrounding surface. In contrast, Magsure 275 showed only limited corrosion localisation near the hole edge, and the overall surface remained free from the severe red rusting observed in GI. This behaviour indicates that the Zn–Al–Mg coating is better able to withstand the combined effects of deformation-induced damage and cyclic corrosive exposure.

Overall, the CCT results after cupping, drawing, and hole expansion deformation clearly demonstrate that Magsure 275 provides significantly better corrosion protection than GI 275 under strained conditions. While both coatings may undergo local coating damage during forming, the deterioration rate of Magsure is substantially lower. This improved post-forming corrosion resistance can be attributed to the multiphase Zn–Al–Mg microstructure, which promotes more stable sacrificial protection and the formation of protective corrosion products, thereby delaying substrate exposure. These findings are particularly important for practical applications in which coated steel sheets undergo severe forming before service, since they confirm that Magsure offers superior durability without sacrificing functional manufacturability.

3.5 Corrosion Performance in Concrete Medium

The corrosion behaviour of the coated steels in the concrete medium revealed a clear difference between GI 275 and Magsure 275, as shown in Figure 8. The measured

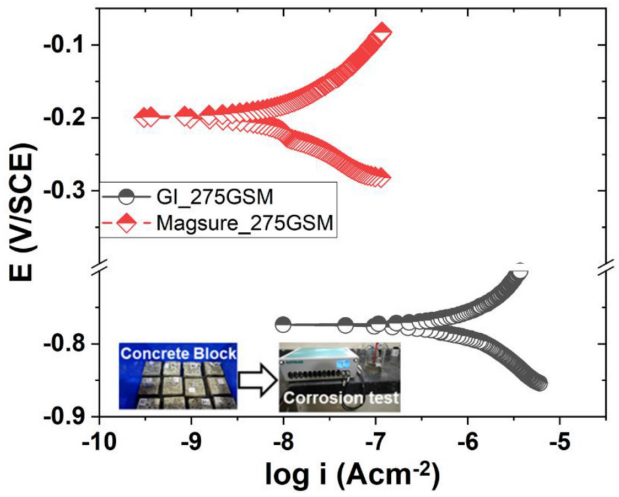


Figure 8. Corrosion performance of GI-275 and Magsure-275 embedded in M40 in a concrete medium and exposed to a chloride environment.

corrosion value for GI 275 was 0.006884 mm/year, whereas Magsure 275 exhibited a significantly lower value of 0.0005 mm/year. This indicates that the corrosion response of Magsure was substantially suppressed under the simulated concrete exposure condition. Quantitatively, the corrosion value of Magsure was nearly 13.8 times lower than that of GI, corresponding to an approximate 92.7% reduction. Such a pronounced improvement confirms the superior protective performance of the Zn–Al–Mg alloy coating in alkaline chloride-bearing concrete environments.

The improved behaviour of Magsure 275 can be attributed to its multiphase Zn–Al–Mg microstructure, particularly the presence of Mg-containing intermetallic/eutectic phases as shown in Figures 2 and 3, which enhance sacrificial protection and promote the formation of more stable and compact corrosion products. These protective products act as an effective barrier against further ingress of corrosive species, thereby reducing the overall corrosion activity. In contrast, the higher value observed for GI 275 indicates relatively faster degradation of the conventional zinc coating under the same exposure conditions. The results therefore demonstrate that Magsure offers a significant durability advantage over GI for applications involving concrete-associated service environments.

4. Conclusion

Based on the microstructural, electrochemical, and corrosion investigations carried out in the present study, the following conclusions are drawn:

- **The Zn–Al–Mg-based Magsure coating exhibited a distinct multiphase microstructure whose morphology evolved systematically with coating mass.** SEM and EDS analyses revealed the presence of primary and eutectic constituents, with increasing coating mass leading to progressive coarsening of the eutectic structure and an increased fraction of Mg-containing phases, which are expected to strongly influence the corrosion behaviour of the coating.
- **XRD analysis confirmed the alloyed phase constitution of Magsure 275, with HighScore-based phase quantification indicating an $MgZn_2$ phase fraction of approximately 26–29%.** In contrast to the Zn-dominant GI 275 coating, the substantial presence of $MgZn_2$ in Magsure 275 establishes the metallurgical basis for its enhanced sacrificial response and improved corrosion resistance.
- **Magsure 275 demonstrated a superior microstructural architecture compared with GI 275, while retaining comparable practical formability.** Although the Magsure coating exhibited significantly higher hardness than GI, its behaviour under cupping, drawing, and hole expansion conditions indicated that the enhanced corrosion resistance was achieved without any major compromise in forming performance.
- **Under all corrosion exposure conditions investigated, Magsure 275 showed markedly better durability than GI 275.** In ASTM B117 salt spray testing, GI 275 exhibited red rust after 960 h, whereas Magsure 275 remained free from red rust even after 4272 h, indicating a corrosion life improvement of at least 4.45 times, with the actual enhancement expected to be greater. Similarly, cyclic corrosion testing after deformation confirmed that Magsure retained significantly better protection than GI under strained conditions.
- **The overall improvement in corrosion performance of Magsure is attributed to the combined effect of its multiphase Zn–Al–Mg coating structure, the presence of the $MgZn_2$ intermetallic phase, and the formation of more stable protective corrosion products during exposure.** The substantially lower corrosion response of Magsure in concrete medium further confirms its suitability for aggressive service environments. Therefore, Magsure can be considered a promising next-generation coated steel for long-life applications requiring both corrosion durability and manufacturing compatibility.

5. Acknowledgements

The authors would like to extend sincere thanks to the advanced corrosion lab and characterisation lab of the Department of Research and Development, JSW Steel Ltd., Vijayanagar Works, for the help and support extended during this study.

6. Declaration of Generative Artificial Intelligence (AI) and AI-assisted Technologies in the Writing Process

During the preparation of this work, the author(s) used ChatGPT to improve the readability and language of the writing. After using this tool, the author(s) reviewed and edited the content as needed and take(s) full responsibility for the content of the published article.

7. References

1. Huang F, Liu Y, Tao X, Wang H, Wang J, Zhang D. Cracking behavior of zinc coating on pre-cracked hot-dip galvanized steel plate under static tension. Structures. 2024; 61:106019. https://doi.org/10.1016/j.istruc.2024.106019
2. Chaouki A, Ben Ali M, El Maalam K, Aouadi K, Benabdallah I, El Fatimy A, Naamane S. Optimizing corrosion protection: Performance comparison of Zn and Zn-Al-Mg alloys hot-dip galvanized coatings. J Alloys Compd. 2024; 1007:176371. https://doi.org/10.1016/j.jallcom.2024.176371
3. He X, Zhou X, Shang T, Liu W, Jiang G, Liu C, Cheng X, Zhang X, Li X. Influence mechanism of different elements and alloy phases on the corrosion resistance of Zn-Al-Mg coated steel in the atmospheric environment: A review. Corros Commun. 2024; 13:49-59. https://doi.org/10.1016/j.corcom.2023.11.001
4. Kim SH, Kim S, Kim HM, Kang J, Lee MH, Oh MS, Yun YS. Enhancing the steam oxidation reactivity of Zn-Al-Mg alloy-coated steel sheets through heat treatment. Appl Surf Sci. 2025; 702:163329. https://doi.org/10.1016/j.apsusc.2025.163329
5. Schürz S, Luckeneder GH, Fleischanderl M, Mack P, Gsaller H, Kneissl AC, Mori G. Chemistry of corrosion products on Zn-Al-Mg alloy-coated steel. Corros Sci. 2010; 52:3271-3279. https://doi.org/10.1016/j.corsci.2010.05.044
6. Volovitch P, Vu TN, Allély C, Abdel Aal A, Ogle K. Understanding corrosion via corrosion product characterization: II. Role of alloying elements in improving the corrosion resistance of Zn-Al-Mg coatings on steel. Corros Sci. 2011; 53:2437-2445. https://doi.org/10.1016/j.corsci.2011.03.016
7. Rai PK, Rout D, Satish Kumar D, Sharma S, Balachandran G. Effect of magnesium on corrosion behavior of hot-dip Zn-Al-Mg coating. J Mater Eng Perform. 2021; 30:4138-4147. https://doi.org/10.1007/s11665-021-05718-z
8. Liu Y, Gu T, Liu M, Wang Z, Cao G, Guo Q, Wang C. Corrosion mechanism of a high corrosion-resistance Zn-Al-Mg coating in typical extremely harsh marine and cold environments. J Mater Res Technol. 2024; 33:4290-4302. https://doi.org/10.1016/j.jmrt.2024.10.080
9. Choi J, Jung EJ, Park DJ, Kim HW, Huh JY, Kim TC, Kim MS. Impact of cooling rates on the microstructure and cracking susceptibility of hot-dip galvanized Zn-12 wt% Al-5 wt% Mg coatings. Surf Coat Technol. 2024; 488:131050. https://doi.org/10.1016/j.surfcoat.2024.131050
10. Nie X, Leyland A, Song HW, Yerokhin AL, Dowey SJ, Matthews A. Thickness effects on the mechanical properties of micro-arc discharge oxide coatings on aluminium alloys. Surf Coat Technol. 1999; 116-119:1055-1060. https://doi.org/10.1016/S0257-8972(99)00089-4
11. Diler E, Lescop B, Rioual S, Nguyen Vien G, Thierry D, Rouvellou B. Initial formation of corrosion products on pure zinc and MgZn2 examinated by XPS. Corros Sci. 2014; 79:83-88. https://doi.org/10.1016/j.corsci.2013.10.029
12. Yao C, Wang Z, Tay SL, Gao W. Effects of Mg on morphologies and properties of hot-dipped Zn-Mg coatings. Surf Coat Technol. 2014; 260:39-45. https://doi.org/10.1016/j.surfcoat.2014.06.067
13. Malla AD, Sullivan JH, Penney DJ, Goldsworthy M, Britton D, Williams G, Goodwin F, Cardoso AP. Mechanistic investigation on the influence of coating weights on the corrosion behaviour of hot-dip-galvanised Zn-Mg-Al coatings. npj Mater Degrad. 2024; 8:78. https://doi.org/10.1038/s41529-024-00494-2
14. Lee JW, Park BR, Oh SY, Yun DW, Hwang JK, Oh MS, Kim SJ. Mechanistic study on the cut-edge corrosion behaviors of Zn-Al-Mg alloy coated steel sheets in chloride containing environments. Corros Sci. 2019; 160:108170. https://doi.org/10.1016/j.corsci.2019.108170
15. Schürz S, Fleischanderl M, Luckeneder GH, Preis K, Haunschmied T, Mori G, Kneissl AC. Corrosion behaviour of Zn-Al-Mg coated steel sheet in sodium chloride-containing environment. Corros Sci. 2009; 51(10):2355-2363. https://doi.org/10.1016/j.corsci.2009.06.019
16. Hosking NC, Ström MA, Shipway PH, Rudd CD. Corrosion resistance of zinc-magnesium coated steel. Corros Sci. 2007; 49(9):3669-3695. https://doi.org/10.1016/j.corsci.2007.03.032
17. Prosek T, Nazarov A, Bexell U, Thierry D, Serak J. Corrosion mechanism of model zinc-magnesium alloys in

atmospheric conditions. Corros Sci. 2008; 50(8):2216-2231. https://doi.org/10.1016/j.corsci.2008.06.008

18. Prosek T, Persson D, Stoulil J, Thierry D. Composition of corrosion products formed on Zn-Mg, Zn-Al and Zn-Al-Mg coatings in model atmospheric conditions. Corros Sci. 2014; 86:231-238. https://doi.org/10.1016/j.corsci.2014.05.016
19. Rodriguez J, Chenoy L, Roobroeck A, Godet S, Olivier MG. Effect of the electrolyte pH on the corrosion mechanisms of Zn-Mg coated steel. Corros Sci. 2016; 108:47-59. https://doi.org/10.1016/j.corsci.2016.02.041
20. Wint N, Cooze N, Searle JR, Sullivan J, Williams G, McMurray H, Luckeneder GH, Riener C. The effect of microstructural refinement on the localized corrosion of model Zn-Al-Mg alloy coatings on steel. J Electrochem Soc. 2019; 166(11):C3147-C3158. https://doi.org/10.1149/2.0171911jes

Author Contribution

H.K.M: Writing – original draft, Writing–review & editing, Conceptualization, Investigation, Methodology, Data curation, Formal analysis, Validation, Visualization; **V.P.:** Investigation, Methodology, Data curation, Validation, Formal analysis, Writing– review & editing; **V.K.Y.:** Investigation, Methodology, Validation, Formal analysis, Writing–review & editing; **K.M.S.S.**: Data curation, Formal analysis; **S.K.**: Writing–review & editing, Validation, Supervision, Resources; **D.S.K.:** Writing–review & editing, Validation, Supervision, Resources, Project administration, Funding acquisition, Conceptualization.